THE JOURNAL OF PHYSICAL CHEMISTRY C

Article

pubs.acs.org/JPCC

Tuning Optical Properties of Al_2O_3/ZnO Nanolaminates Synthesized by Atomic Layer Deposition

Adib Abou Chaaya,[†,∥] Roman Viter,[*,‡,§,∥] Ieva Baleviciute,[⊥] Mikhael Bechelany,[*,†] Arunas Ramanavicius,[⊥] Zanda Gertnere,[§] Donats Erts,[§] Valentyn Smyntyna,[‡] and Philippe Miele[†]

[†]Institut Europeen des Membranes, IEM, ENSCM-UM2-CNRS, UMR 5635, Universite Montpellier 2, Place Eugene Bataillon, F-34095, Montpellier cedex 5, France

[‡]Faculty of Physics, Experimental Physics Department, Odessa National I. I. Mechnikov University, 42, Pastera, 65026, Odessa, Ukraine

[§]Institute of Chemical Physics, University of Latvia, 19, Raina Boulevard, LV 1586, Riga, Latvia

[⊥]Faculty of Chemistry, Department of Physical Chemistry, Vilnius University, Naugarduko 24, 03225 Vilnius 6, Lithuania

Supporting Information

ABSTRACT: Nanolaminates are of great interest for their unique properties such as high dielectric constants and advanced mechanical, electrical, and optical properties. Here we report on the tuning of optical and structural properties of Al_2O_3/ZnO nanolaminates designed by atomic layer deposition (ALD). Structural properties of nanolaminates were studied by SEM, GIXRD, and AFM. Optical characterization was performed by transmittance and photoluminescence (PL) spectroscopy. Complex study of monolayer properties was performed by ellipsometry. Optical constants for Al_2O_3 and ZnO monolayer were calculated. The band gap of ZnO single layers and the excitonic PL peak position were shifted to the UV region related to quantum confinement effects. No peaks in the UV region were observed in nanolaminates with 2 nm ZnO single layer thickness due to fully depleted region in small crystalline grains (<2 nm). The improved room temperature photoluminescence of nanolaminates makes them prominent materials for optical biosensors applications.

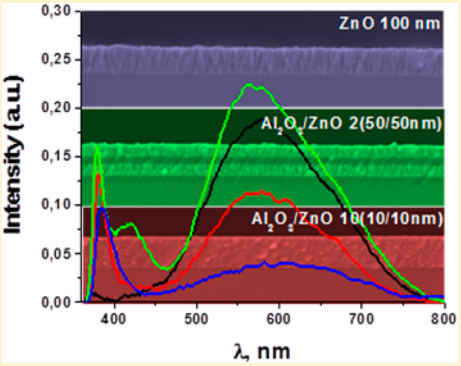

INTRODUCTION

In the past decade, the attention of researchers has been given to the design of new nanoscale materials with advanced properties. One of these nanostructures is nanolaminates formed by alternating layers of different materials, which have individual layer thicknesses on the nanometer scale.[1−3] These multilayered structures often demonstrate unique properties such as high dielectric constants and advanced mechanical,[4−6] electrical, and optical properties. The latter depends on the constituent materials forming the nanolaminates.[1−3] Among these materials, zinc oxide, an n-type semiconductor with wide band gap value (3.3 eV) and high exciton binding energy (0.06 eV), demonstrates room temperature photoluminescence in the UV−vis region.[7] Electrical and optical properties of ZnO can be tailored by doping[8] using, for instance, aluminum or/and aluminum oxide (Al_2O_3).[9−14] Quantum confinement effects in ZnO can appear in the case of the encapsulation into a dielectric core,[15−18] changing electrical, dielectric, and optical properties. Due to this, ZnO ultrathin layers (thickness less than 50 nm) surrounded by a dielectric media, formed by Al_2O_3, for instance, are expected to demonstrate quantum confinement effects.

Atomic layer deposition (ALD) is a powerful tool to fabricate different oxide materials.[19] Due to two self-limiting surface reactions, ALD allows growing pinhole free, continuous, smooth, and substrate conformal ultrathin film as well as multilayered films with precise dimensional control at the subnanometer level. Different studies report the growth of Al_2O_3/ZnO nanolaminates as well as the incorporation of Al doping in ZnO using ALD.[4−6,20,21] The comparison between ZnO pure thin film and Al_2O_3/ZnO nanolaminates shows that the ZnO changes its growth direction when deposited on Al_2O_3 layer.[10] Al_2O_3 thin films deposited by ALD are amorphous in nature independently of their thickness, whereas ZnO nanolayers show a transition from amorphous to nanocrystalline phases when bilayer spacing increased.[6] Thin amorphous Al_2O_3 layers work as stopping layers for ZnO crystal growth.[22]

The investigation of optical properties of Al-doped ZnO showed the increase of band gap as a function of Al doping concentration varying from 3.28 to 3.7.[10,11] This blue shift of band gap has been attributed to the Al doping of ZnO layers (Burstein−Moss effect) as well as to the quantum confinement effects.[10,11] Wang et al.[23] demonstrate that Al_2O_3 buffer layer led to an increase of the near band edge emission (NBE) and a

Received: December 6, 2013
Revised: January 31, 2014
Published: January 31, 2014

   dx.doi.org/10.1021/jp411970w | J. Phys. Chem. C 2014, 118, 3811−3819

decrease of a deep level emission (DLE). The ratio of NBE/DLE intensities was above 60. The DLE quenching of the ZnO films growing on Al_2O_3 buffer layer was attributed to the decrease of oxygen vacancies concentration on the interfacial layer. The proposed model supposed that the oxygen atoms are removed from the amorphous Al_2O_3 layer and occupy the oxygen vacancies at the initial stage of the growth of ZnO films to improve its crystallization.[23] Recently, Karvonen et al.[22] demonstrated the enhancement of the third-order optical nonlinearity in ZnO/Al_2O_3 nanolaminates fabricated by ALD.

In the present paper, we report structural and optical properties of Al_2O_3 nanolaminates, fabricated by ALD method. Single layer parameters (thickness, grain size, refractive index, extinction coefficient, and band gap) were calculated. The mechanism of formation of nanolaminates and Al penetration into ZnO layer was proposed. Blue shift of the band gap with the decrease of the bilayer Al_2O_3/ZnO thickness in the nanolaminate is observed. Room temperature photoluminescence shows the modification of the excitonic PL of ZnO dependent on the thickness of bilayer. Mechanisms of blue shift of the band gap and PL changes of nanolaminates are discussed in light of the quantum confinement effect and the Al doping as well as the improvement of crystallinity of the nanolaminates.

MATERIALS AND METHODS

Synthesis of Al_2O_3/ZnO Nanolaminates by ALD. Diethyl zinc (DEZ) ($Zn(CH_2CH_3)_2$, 95% purity, CAS: 557-20-0) and trimethylaluminum (TMA) ($(CH_3)_3Al$) 98% purity, CAS: 75-24-1) were purchased from Sigma Aldrich. Silicon wafer p-type (100) was obtained from MEMC Korea company and glass substrates from RS France. Substrates were precleaned in acetone, ethanol, and deionized water for 5 min to remove organic contaminants. A custom-made ALD reactor was used for the synthesis of Al_2O_3/ZnO multilayers. ALD was performed using sequential exposures of TMA (DEZ) and H_2O separated by a purge of nitrogen with a flow rate of 100 sccm. The deposition regime for ZnO and Al_2O_3 consisted of a 0.1 s pulse of DEZ (TMA), 30 s of exposure to DEZ (TMA), 30 s of purge with nitrogen followed by 2 s pulse of H_2O, 30 s of exposure to H_2O, and finally 40 s purge with nitrogen. ZnO thin films as well as Al_2O_3/ZnO nanolaminates with different numbers of cycles were deposited on both Si substrates and glass substrates by ALD (Table 1), and the temperature was fixed to 100 °C.

Characterization. Structural properties of Al_2O_3/ZnO nanolaminates were characterized by scanning electron microscopy (SEM; Hitachi S-4800 microscope) and grazing incidence X-ray diffraction (GIXRD; Bruker D5000). The surface morphology was studied by Asylum Research MFP-3D atomic force microscope, operating in tapping mode and equipped with a commercial silicon tip. The size of the AFM images was 3 μm × 3 μm. The thicknesses of ZnO and Al_2O_3 layers were measured using SEM and ellipsometry.

Optical properties of ZnO thin films have been studied with UV−vis transmittance (UV−vis spectrophotometer Shimadzu UV-1700, spectral range 300−1100 nm, 1 nm step) and photoluminescence spectroscopy (spectral range 370−800 nm). The excitation of luminescence was performed by a solid state laser source (Nd:YAG, LCS-DTL-374QT, Russia, 355 nm, 13 mW/cm^2). The registration of the emitted spectra was provided by an experimental setup described elsewhere.[24]

For spectroscopic ellipsometry measurements, spectral ellipsometer M-2000X from J.A.Woollam (U.S.A.) with a rotating compensator operating in the spectral range from 200 to 1000 nm was used. All measurements were performed at fixed angle of incidence at 70°. For regression analysis Complete Ease software from J. A. Woollam was used.

Table 1. ALD ZnO Single Thin Film and Al_2O_3/ZnO Nanolaminate Synthesis

samples	cycles of Al_2O_3	cycles of ZnO	numbers of bilayers	bilayer thickness (nm)
Al_2O_3/ZnO 50 (2/2 nm)	10	10	50	4
Al_2O_3/ZnO 10 (10/10 nm)	50	50	10	20
Al_2O_3/ZnO 2 (50/50 nm)	250	250	2	100
ZnO 100 nm	–	500	–	–

RESULTS AND DISCUSSION

Design of Nanolaminates. Figure 1a shows cross-sectional SEM images of ZnO thin film of 100 nm thickness and two illustrative examples of Al_2O_3/ZnO nanolaminates with different sequences. The SEM images indicate a conformal coating by ALD of the Si substrate in both cases. The SEM cross section proves as well that the sequence of alternating Al_2O_3 and ZnO interlayers was achieved throughout the total film thickness of the nanolaminates. In all nanolaminates, the first layer on Si substrate was Al_2O_3, and the top layer of the nanolaminate was ZnO. The SEM images show that the single layer of ZnO developed a rough surface of columnar growth where the nanolaminates consist of alternating layers of amorphous Al_2O_3 and nanocrystalline ZnO.[6,23] The growth rates of Al_2O_3 and ZnO in the nanolaminates vary from 1.4 to 2 Å per cycle and 1.8 to 2 Å per cycle, respectively, as it has been determined elsewhere.[6]

The EDX of nanolaminates Al_2O_3/ZnO 10 (10/10 nm) consisting of alternating ZnO/Al_2O_3 films (Figure 1b) grown at 100 °C by ALD showed the presence of Al, Zn, and O. GIXRD patterns of Al_2O_3/ZnO nanolaminates are shown in Figure 1c. The Al_2O_3/ZnO 50 (2/2 nm) nanolaminates with the thinnest bilayer thickness showed weak broad X-ray diffraction peak at 34.26° which can result from their amorphous structure or their crystalline size below 2 nm.[25] The increase of the bilayer thickness in the nanolaminates, Al_2O_3/ZnO 10 (10/10 nm), led to the appearance of XRD peaks at 2θ = 31.82° and 34.35° and a weak peak at 2θ = 36.1° corresponding to (100), (002), and (101) reflections of ZnO, respectively. For thicker bilayer thickness, Al_2O_3/ZnO 2 (50/50 nm), strong peaks at 2θ = 31.74° and 34.35° have been observed. The XRD peak at 36.1−36.2° appeared in both spectra for thick bilayers in the nanolamiantes but with rather low intensity. A change in the preferential growth orientation (strong (002) and negligible (101) XRD peaks) is observed when comparing the thicker nanolaminate Al_2O_3/ZnO 2 (50/50 nm) to the single ZnO film (100 nm). No peaks related to Al_2O_3 were observed.

From these XRD spectra, lattice constants and d-spacing between the atomic planes for ZnO single films and Al_2O_3/ZnO nanolaminates with different sequences were calculated. The lattice constant (a) increased when the bilayers thickness in the nanolaminates enhanced, whereas the lattice constant (c) decreased at the same time. The lattice constant (a) was lower than the similar value for ZnO (i.e., 100 nm thick: Table 2),[26] but the lattice constant (c) was higher than for ZnO (i.e., 100

dx.doi.org/10.1021/jp411970w | J. Phys. Chem. C 2014, 118, 3811−3819

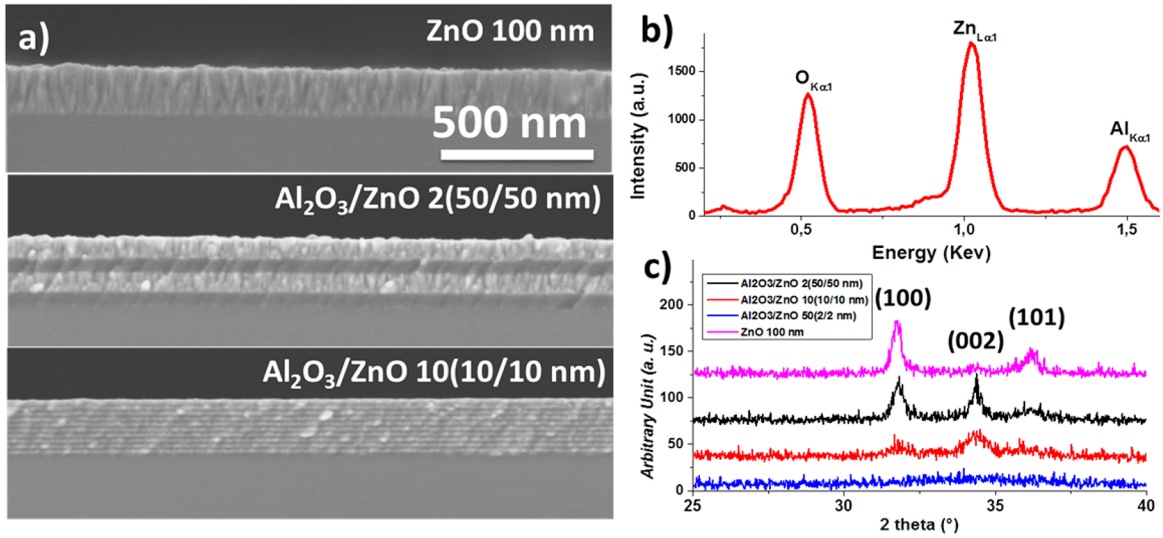

Figure 1. SEM images of ZnO thin film of 100 nm thickness and Al_2O_3/ZnO nanolaminates with different sequences (a) EDX of Al_2O_3/ZnO nanolaminates (b) and GIXRD of ZnO thin film of 100 nm thickness and Al_2O_3/ZnO nanolaminates with different sequences (c).

Table 2. Lattice Constant, *d*-Spacing, and Texture Coefficient of ZnO Single Thin Film of 100 nm Thickness and Al_2O_3/ZnO Nanolaminates with Different Bilayer Thicknesses

	Al_2O_3/ZnO 50 (2/2 nm)	Al_2O_3/ZnO 10 (10/10 nm)	Al_2O_3/ZnO 2 (50/50 nm)	ZnO (100 nm)
		Lattice Constant		
a (nm)	–	0.3244 ± 0.0006	0.3247 ± 0.0004	0.3253 ± 0.0005
c (nm)	0.523 ± 0.0006	0.5218 ± 0.0004	0.5215 ± 0.0005	0.5213 ± 0.0002
		d-Spacing		
d(100) (nm)	–	0.2809	0.2812	0.2849
d(002) (nm)	0.2615	0.2609	0.2607	0.2606
d(101) (nm)	–	0.2481	0.2485	0.2478
		Texture Coefficient		
[100]	–	0.66	1.28	1.66
[002]	–	2.07	1.52	0.237396
[101]	–	0.27	0.20	0.468436

nm: Table 2). As a result, for Al_2O_3/ZnO 2 (50/50 nm) and Al_2O_3/ZnO 10 (10/10 nm), the *d*-spacing (100) is lower than for ZnO single layer (i.e., 100 nm: Table 2), whereas for the *d*-spacing (002), it is a bit higher than for ZnO single layer. We note that the *d*-spacing (101) was lower for Al_2O_3/ZnO 2 (50/50 nm) and Al_2O_3/ZnO 10 (10/10 nm) than for ZnO (i.e., 100 nm thick: Table 2).[26]

Texture coefficients (TC) calculated for the nanolaminates samples with different sequences, according to Marquez et al.,[27] match the preferred growth orientation in the (002) direction. In thicker bilayers (Al_2O_3/ZnO 2 (50/50 nm)), lateral growth in the (100) direction was observed (TC = 1.28).

Grain size was estimated from the Scherer equation for thick bilayers thicknesses Al_2O_3/ZnO 10 (10/10 nm) and Al_2O_3/ZnO 2 (50/50 nm)[28,29]

$$D = \frac{0.9\cdot\lambda}{\beta\cdot\cos(\theta)} \quad (1)$$

where λ, β, and θ are X-ray wavelength, full width at half-maximum (fwhm), and diffraction angle, respectively. The grain size of Al_2O_3/ZnO 50 (2/2 nm) nanolaminates has been estimated from TEM measurement reported elsewhere.[6] The obtained grain size values were ∼2, 7, and 14 nm for Al_2O_3/ZnO 50 (2/2 nm), Al_2O_3/ZnO 10 (10/10 nm), and Al_2O_3/ZnO 2 (50/50 nm), respectively.

From these observations, we can conclude that in the first stage, vertical growth of ZnO on amorphous Al_2O_3 is initiated. At low bilayer thickness Al_2O_3/ZnO 50 (2/2 nm), wurzite ZnO with low crystalline quality was observed. The lattice parameter (*c*) increased, matching possible interstitial Al incorporation in ZnO structure at least at the interface between ZnO and Al_2O_3.[12] The thickness of doped layer of ZnO might be in the range of 0.1−1 nm as the increase of the bilayer thickness from 4 to 100 nm in the nanolaminates turned back the lattice constants of the ZnO to the values which characterize single ZnO film.

Surface morphology of the samples was studied using the AFM method (Figure 2a). Samples with low bilayer thickness Al_2O_3/ZnO 50 (2/2 nm) and Al_2O_3/ZnO 10 (10/10 nm) showed smooth surface with insignificant surface roughness. Well-shaped hill-shaped features with average lateral dimensions 50−100 nm have been observed on the Al_2O_3/ZnO 2 (50/50 nm) sample surface. The mean square roughness, calculated from AFM data, showed linear behavior vs the increase of bilayer thickness (Figure 2b). The obtained results are consistent with that published by Elam et al.[21] Amorphous Al_2O_3 blocks the ZnO crystal growth and forces the ZnO to renucleate on the Al_2O_3 surface. We note that surface roughness of nanolaminates was lower than that for 200 nm thick ZnO (Figure 2b).[26]

dx.doi.org/10.1021/jp411970w | J. Phys. Chem. C 2014, 118, 3811−3819

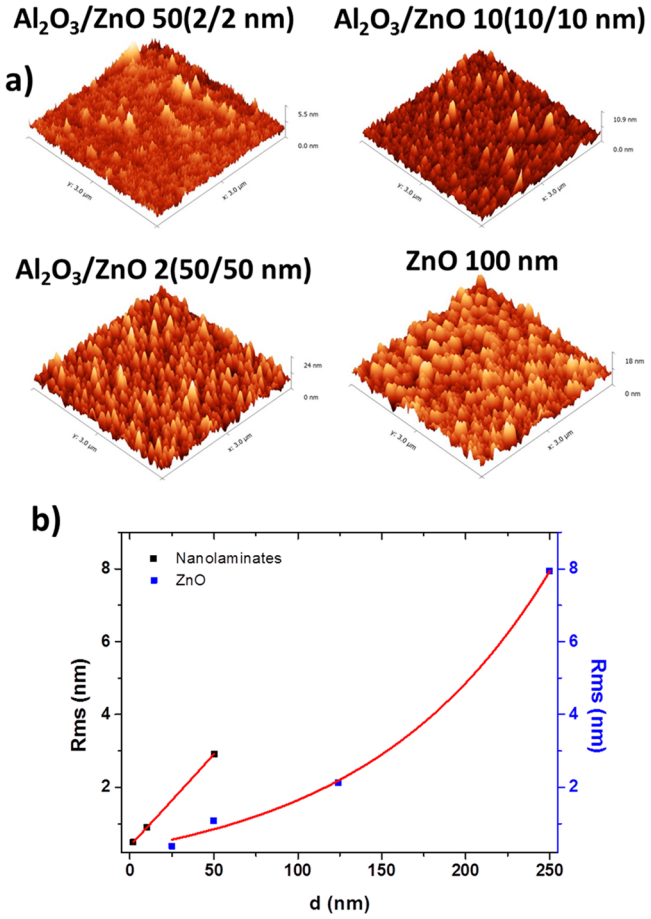

Figure 2. (a) AFM images of Al_2O_3/ZnO nanolaminates with different bilayer thicknesses and ZnO thin film of 100 nm thickness (b) Blue square, roughness vs the film thickness of single layer of ZnO; black square, roughness vs the top layer of ZnO in the Al_2O_3/ZnO nanolaminates.

Optical Properties. *Transmittance.* Transmittance spectra of Al_2O_3/ZnO nanolaminates are shown in Figure 3a. All measured samples were transparent in the range of 550−1100 nm. The absorption edge of the samples was found in the region of 370−410 nm. Blue shift of absorption edge was observed particularly with the decrease of nanolaminate bilayer thickness. The band gap value of the samples was calculated considering that Al_2O_3 was totally transparent and the observed absorption edge was related to ZnO layers. ZnO is known as a semiconductor with direct optical transitions. Therefore, the absorption coefficient α can be described by the following equation[30]

$$\alpha = \frac{(h\nu - E_g)^2}{h\nu} \tag{2}$$

where $h\nu$ and E_g are photon energy and band gap values, respectively. Absorption coefficient α is related to the transmittance of the sample T as

$$\alpha \cdot d = \ln\left(\frac{1}{T}\right) \tag{3}$$

where d is a thickness of the sample.

In order to simplify the calculation of the band gap values of the nanolaminates, an optical density OD (OD = $\alpha \times d$) was used. Considering eq 2 and eq 3, the plot $(\mathrm{OD} \times h\nu)^2$ vs $h\nu$ was obtained (Figure 3b). Band gap values E_g were graphically calculated in the linear part of the absorption edge with respect to eq 2 (Figure 3b) and are summarized in Table 3.

Table 3. Band Gap of Al_2O_3/ZnO Nanolaminates with Different Bilayer Thicknesses and ZnO Single Thin Film of 50 nm Thickness

	E_g (eV) from transmittance	E_g (eV) from ellipsometry
Al_2O_3/ZnO 50 (2/2 nm)	3.41	3.45
Al_2O_3/ZnO 10 (10/10 nm)	3.3	3.36
Al_2O_3/ZnO 2 (50/50 nm)	3.28	3.31
ZnO (50 nm)	3.24	3.25

The band gap increased with the decrease of the bilayer thickness in the nanolaminates. The obtained E_g values can be affected by structural defects (interstitials, vacancies, etc.) and impurities. The observed blue shift could be determined by three physical phenomena:[31,32] (i) quantum confinement effect

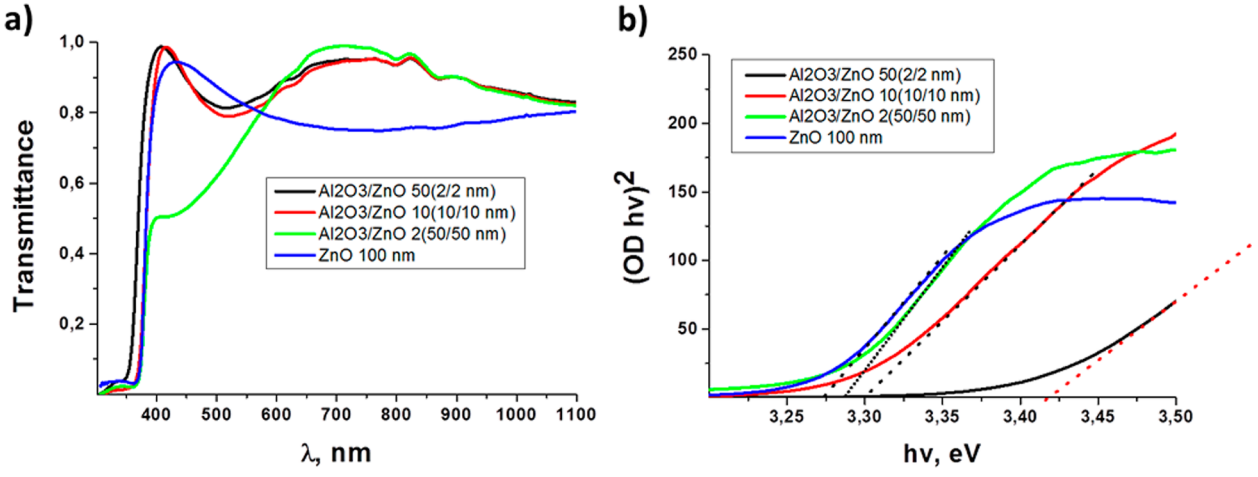

Figure 3. (a) Transmittance spectra and (b) band gap estimation of Al_2O_3/ZnO nanolaminates with different bilayer thickness and single ZnO thin film.

dx.doi.org/10.1021/jp411970w | J. Phys. Chem. C 2014, 118, 3811−3819

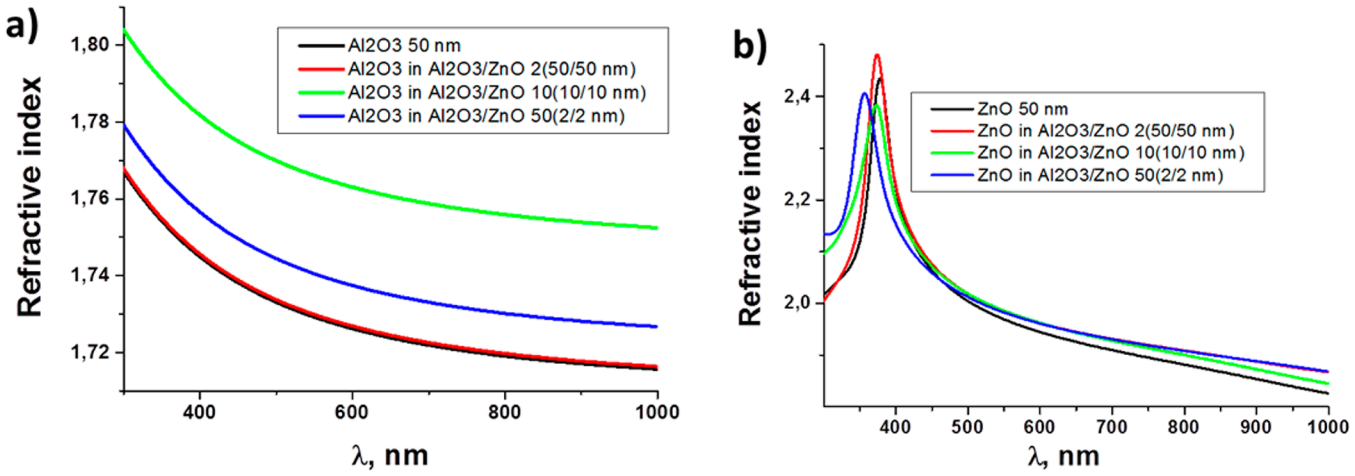

Figure 4. (a) Refractive index (real part) of Al_2O_3 single thin film and Al_2O_3 in Al_2O_3/ZnO nanolaminates with different bilayer thicknesses. (b) Refractive index (real part) of ZnO single thin film and ZnO in Al_2O_3/ZnO nanolaminates with different bilayer thicknesses.

of small nanograins, (ii) doping of ZnO by Al, and (iii) improvement of crystalline quality of the single layer.

In our previous work,[26] we reported E_g and crystalline values of pure ZnO single layers deposited by ALD. ZnO samples (thickness 50 nm) were nanocrystalline with 6 nm of grain size and a band gap about 3.24 eV. We also showed that E_g value increased from amorphous to nanocrystalline samples.[26] As was mentioned before, the Al_2O_3 layer stimulates ZnO growth and improves the crystallinity of the films. However, the grain size of Al_2O_3/ZnO 2 (50/50 nm) nanolaminates was twice as high compared with the 50 nm thick layer of ZnO. Considering this fact, we suppose that the blue shift, which is related to the size effects, can occur only for nanolaminates with bilayer thickness of 4 nm. For other samples, which were based on 20 and 100 nm thick bilayers, the doping by Al and improvement of the crystalline structure are the most plausible explanations for observed blue shift.[10,11]

Spectroscopic Ellipsometry. Spectroscopic ellipsometry has been applied for the investigation of the thickness and the optical constants (refractive index and extinction coefficients) of single ZnO and Al_2O_3 layers as well as the evaluation of nanolaminates (Figure 4). The regression analysis was performed applying different types of models. ZnO layer was characterized using Psemi−MO and two Gausian oscillators from "Complete Ease" software. For characterization of Al_2O_3 layers, the Cauchy dispersion function was selected. It is commonly used for transparent materials as dielectrics and semiconductors. First, optical constants and layer thickness of single Al_2O_3 and ZnO layers deposited on Si substrate were obtained. It was done by fixing the thickness value and fitting the dispersion function. The values of Cauchy function used for Al_2O_3 characterization coefficients $A = 1.716$, $B = 2.36 \times 10^{-2}$, and $C = 1.57 \times 10^{-3}$ and a thickness of layer ($d = 40.81$ nm) were determined from regression analysis. This optical constant value is close to that reported by Barker et al. on α-$A1_2O_3$ lattice belonging to the trigonal crystal system.[33] The single layer of ZnO optical constants and layer thickness ($d = 48.63$ nm) were obtained from regression analysis with the following Psemi−Mo oscillator values: Amp1 = 2.542, Br1 = 0.0798, Eo1 = 3.288, WR1 = 2.2419, PR1 = 0.631, AR1 = 0.542, O2R1 = −0.565; Gaussians oscillator values were Amp2 = 2.53, Br2 = 2.53, En2 = 6.47, Amp3 = 0.265, Br3 = 0.46, En3 = 0.885. The calculated optical constants of ZnO nanolayers obtained by ALD are in good agreement with ZnO having hexagonal crystals structure reported by Dai et al.[34]

In order to study the optical response of ellipsometric parameters of multilayer system (nanolaminates) composed of Al_2O_3 and ZnO layers deposited by ALD method during regression analysis, the thicknesses of layers were fixed parameters; meanwhile, coefficients in optical dispersion functions were free fitting values. As noted above, the obtained optical constants for single Al_2O_3 and ZnO layers were used as a starting point for the regression analysis based evaluation of ZnO/Al_2O_3 nanolaminates.

For the Al_2O_3/ZnO 50 (2/2 nm) nanolaminate, the Bruggeman effective media approach was used for regression analysis. First, the total thickness was obtained in a range from 400 to 1000 nm. After that the coefficients of optical constants functions were fitted in spectral range from 300 to 1000 nm to evaluate the peculiarity in the UV range. Bruggeman's effective media approximation model gives the possibility of evaluating the percentage of materials from which the layer consists and usually is used for the evaluation of polycrystalline materials. After the fitting of percent's in effective media model, using Complete Ease software, it was calculated that the part of Al_2O_3 takes 54.9% and ZnO 45.1% of total volume. We note here that due to the roughness of the interface between layers, the ultrathin (about 2 nm) layer's fluctuations can be of the same order as the thickness of this layer. It can be seen from XRD measurements that the amorphous layers have thickness below 2 nm. This means that such nanolaminates are closer to the dispersed system than to the regular one. Thus, the effective medium approach could be a good enough tool for calculation of the effective refractive index. Since the exact shape of such fluctuations is unknown, the Bruggeman approach is most preferable because it is better to use it in the case of the absence of any independent information about microstructure and in describing film roughness and intermixed layer effects.[35,36] However, the investigation of nanolaminates using He-ion microscope reported elsewhere had demonstrated layered structure of the total film.[6] In order to estimate the error which could be generated due to this anisotropic structure, we used a linear approach of effective medium and Hashin−Shtrikman limit[37] with known volume fractions of the components (55%/45%). This estimation showed that the difference between dielectric constants along and perpendicular

dx.doi.org/10.1021/jp411970w | J. Phys. Chem. C 2014, 118, 3811−3819

to the nanolaminate structures is only 0.1%. This demonstrates that our choice of Bruggeman effective medium approach is able to give accurate enough results.

The main parameters of single ZnO and Al_2O_3 layers (refractive index n and extinction coefficient k) were calculated from ellipsometry measurements. It was found that Al_2O_3 was transparent in the whole UV and vis range of the wavelength (Figure 4a). We note here that ellipsometry allows obtaining the optical constants n (real part of refractive index) and k (imaginary part of refractive index). This was used in the present paper: n vs wavelength was plotted to analyze correlation with the structural properties. However, no drastic changes in n values were observed when we plot n, sqrt($n^2 - k^2$), and sqrt($n^2 + k^2$) in the UV−vis range (Figure SI2 of the Supporting Information).

ZnO single layer demonstrated an absorption peak in the range from 360 to 410 nm (Figure 4b). It is known that extinction coefficient k and absorption coefficient α are related as[38]

$$\alpha = \frac{4 \cdot \pi \cdot k}{\lambda} \quad (4)$$

where λ is a wavelength. Using eqs 2 and 4, band gap values of ZnO single layer were calculated (Table 3). The calculated E_g values were similar to the ones obtained by transmittance spectroscopy (see Figure 3b). It was found that average refractive index of ZnO single layer in nanolaminates was higher than that for the single ZnO films. No drastic changes in refractive index of ZnO in nanolamitates were observed in the range of 450−700 nm. The peak between 350 and 400 nm corresponds to the band gap transition of ZnO.[39] Blue shift of the peaks in dispersion curves ($n(\lambda)$) were observed with the decrease of the single ZnO layer thickness in nanolaminates due to grain size decrease, doping by Al, or the improvement of the crystalline quality.[39] The observed blue shift peak is in good correlation with the calculated band bap values.

Doping of ZnO by Al resulted in changes of optical properties, such as band gap and refractive index.[40,41] It was shown that refractive index of ZnO doped by Al decreased with the concentration ratio of Al-dopant.[40,41] The observed results of refractive index of ZnO showed the increase of refractive index in comparison to single ZnO films. Recently we demonstrated that 50 nm ZnO film on Si was barely nanocrystalline with average grain size of about 6 nm.[26] It was considered that shift of the refractive index is related to the packing density of the film:[40,42,43] as the packing density increases, the n value increases.[40,42,43] In fact, the packaging density (density per volume) is related to the microstructure of the films. The higher the packing density, the less moisture/voids are inside ZnO thin film. ZnO has a columnar microstructure, and a columnar growth is proved. When we deposited ZnO on Al_2O_3, lateral growth can take place. The deviation from the columnar growth can change then the microstructure and increase the packing density and the refractive index as reported by Krishna et al.[44]According to the XRD analysis, the larger grain size in nanolaminates increased with the bilayers thickness. It might be considered that no significant doping occurred in ZnO single layers, but the increase of refractive index of ZnO was based on improved crystalline properties. We suppose that the Al doping at the ZnO/Al_2O_3 interface did not influence the refractive index of ZnO layers.

The refractive index of Al_2O_3 single layer in nanolaminates increased in comparison to single layer of Al_2O_3 deposited on Si (Figure 4b). This layer had amorphous structure.[6] In the present work Al_2O_3 also had amorphous nature as no XRD peaks related to this material were observed. This result is not fully understood yet; however, we could consider the improvement of the structure in amorphous Al_2O_3, similar to ZnO, which resulted in the increase of the refractive index and/or the Zn incorporation at the ZnO/Al_2O_3 interface.

Photoluminescence Spectra. Photoluminescence spectra of nanolaminates are shown in Figure 5, demonstrating UV and

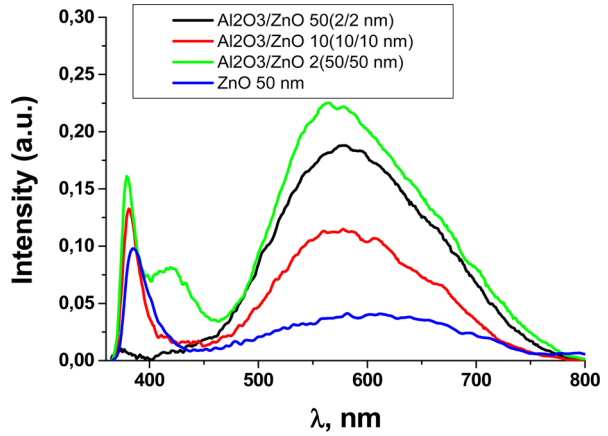

Figure 5. Photoluminesacnce spectra of 50 nm thick single ZnO film and Al_2O_3/ZnO nanolaminates with different bilayer thicknesses.

vis emission bands usually observed in ZnO nanostructures. The UV peak corresponds to free exciton emission, and the vis peak is observed due to defect level emission.[23] The intensity of UV peak increased with the increase of the bilayer thickness in the nanolaminates. The intensity of the vis band does not follow the same tendency. The ratio of UV/vis emission could be a parameter of the crystalline structure quality of ZnO inside the nanolaminates.[45,46]

The low intensity of UV in Al_2O_3/ZnO 50 (2/2 nm) could be effected by high surface-to-volume ratio of the nanocrystalline ZnO. Ábrahám et al.[47] showed that in ZnO quantum dots the UV/vis ratio increased with the quantum dot (QD) radius. The low intensity of UV emission of QD could be attributed to the domination of the surface defect irradiative recombination and the separation of photogenerated charges between volume and surface of QD.[48]

The PL spectra of the nanolaminates were analyzed by Origin 7.0 software by splitting the spectra on separate peaks with the Gaussian fitting (Supporting Information, Figure SI1). The obtained data are presented in the Table 4. Excitonic peaks at 377−378 nm and phonon replicas at 386−388 nm fit well

Table 4. Peak Positions of ZnO Single Thin Film and Al_2O_3/ZnO Nanolaminates with Different Bilayer Thicknesses

Al_2O_3/ZnO 50 (2/2 nm)	Al_2O_3/ZnO 10 (10/10 nm)	Al_2O_3/ZnO 2 (50/50 nm)	ZnO (50 nm)
425.3	380	378	382
560.5	389	386	391
653.1	414	417	406
–	566	552	518
–	660	637	619

dx.doi.org/10.1021/jp411970w | J. Phys. Chem. C 2014, 118, 3811−3819

with the previously published results.[49−52] Peaks at 413−425 nm could be induced by neutral Zn vacancies and/or surface defects.[49−52] Peaks at 536−565 and 635−656 nm correspond to oxygen vacancies and the interstitial oxygen.[53]

It was mentioned that UV/vis intensity of nanolaminates did not increase monotonically with the increase of the single layer thickness (Figure 5). It could be affected by structural changes during the layer growth and/or doping by Al. Yogamalar et al.[30] demonstrated that Al^{3+} ions could substitute Zn^{2+} and therefore Zn vacancies are formed, which are increasing the visible PL band. Additionally, Al doping results in the increase of the electron concentration which could stimulate the defect-based luminescence.[30] Doping by Al also stimulated the formation of surface defects, which could be luminescence centers as well.[30]

Additional defects at Al_2O_3/ZnO interface could be formed, which is confirmed by a relatively strong peak at 413 nm (Figure 5). It was shown that peaks at 413−426 were related to neutral Zn vacancies or/and Zn interstitials.[53−55] Because no doping by Al was approved with ellipsometry and XRD measurements, the increase of the peak intensity could be the result of higher concentration of Zn vacancies/Zn interstitials at Al_2O_3/ZnO interface, as described above.

The obtained nanolaminates were biocompatible and suitable for surface modification. At room temperature, enhanced photoluminescence of Al_2O_3/ZnO 50 (2/2 nm) could be exploited as a platform for the development of new optical sensors and biosensors.

CONCLUSION

In conclusion, optical and structural properties of Al_2O_3/ZnO nanolaminates deposited by ALD are reported. The ALD methods allow the tailoring of structural and optical parameters of the nanolaminates, including single layer thickness, grain size, band gap, and PL. From analysis of optical and structural properties, it was determined that during the synthesis, the formed ZnO single layer in the nanolaminates was not doped by Al. The possible mechanism of nanolaminate formation implies that Al diffused into the interface of ZnO/Al_2O_3 bilayer, forming defect states which increased visible band of PL. Blue shift of band gap and excitonic peak position of ZnO single layers were explained by quantum confinement effect and the improvement of crystalline quality of ZnO layer. The advanced properties of the nanolaminates such as biocompatibility, easy surface modification, and enhanced photoluminescence at room temperature could provide good capacity for the development of nanolaminates-based optical sensors and biosensors.

ASSOCIATED CONTENT

Supporting Information

PL measurement of ZnO ALD films and Al_2O_3/ZnO nanolaminates with different bilayer thicknesses (Figures S1 and S2). This material is available free of charge via the Internet at http://pubs.acs.org.

AUTHOR INFORMATION

Corresponding Authors

*E-mail viter_r@mail.ru; phone +380676639327 (R.V.).
*E-mail mikhael.bechelany@univ-montp2.fr; phone +33467149167; fax +33467149119 (M.B.).

Author Contributions

‖A.A. and R.V. contributed equally to this work.

Notes

The authors declare no competing financial interest.

ACKNOWLEDGMENTS

We are thankful for the financial support by the European Commission through project BIOSENSORS-AGRICULT (PIRSES-GA-2012-318520) and FOTONIKA-LV (FP7-RegPot-2011-1, contract no. 285912).

REFERENCES

(1) Freyman, C. A.; Chung, Y.-W. Synthesis and Characterization of Hardness-Enhanced Multilayer Oxide Films for High-Temperature Applications. *Surf. Coat. Technol.* **2008**, *202* (19), 4702−4708.
(2) Rowlette, P. C.; Wolden, C. A. Pulsed Plasma-Enhanced Chemical Vapor Deposition of Al_2O_3−TiO_2 Nanolaminates. *Thin Solid Films* **2010**, *518* (12), 3337−3341.
(3) Seo, S.-W.; Jung, E.; Chae, H.; Cho, S. M. Optimization of Al_2O_3/ZrO_2 Nanolaminate Structure for Thin-Film Encapsulation of OLEDs. *Org. Electron.* **2012**, *13* (11), 2436−2441.
(4) Abou Chaaya, A.; Le Poitevin, M.; Cabello-Aguilar, S.; Balme, S.; Bechelany, M.; Kraszewski, S.; Picaud, F.; Cambedouzou, J.; Balanzat, E.; Janot, J.-M.; et al. Enhanced Ionic Transport Mechanism by Gramicidin A Confined inside Nanopores Tuned by Atomic Layer Deposition. *J. Phys. Chem. C* **2013**, *117* (29), 15306−15315.
(5) Cabello-Aguilar, S.; Balme, S.; Abou Chaaya, A.; Bechelany, M.; Balanzat, E.; Janot, J.-M.; Pochat-Bohatier, C.; Miele, P.; Dejardin, P. Slow Translocation of Polynucleotides and Their Discrimination by Alpha-Hemolysin inside a Single Track-Etched Nanopore Designed by Atomic Layer Deposition. *Nanoscale* **2013**, *5* (20), 9582−9586.
(6) Raghavan, R.; Bechelany, M.; Parlinska, M.; Frey, D.; Mook, W. M.; Beyer, A.; Michler, J.; Utke, I. Nanocrystalline-to-Amorphous Transition in Nanolaminates Grown by Low Temperature Atomic Layer Deposition and Related Mechanical Properties. *Appl. Phys. Lett.* **2012**, *100* (19), 191912.
(7) Khranovskyy, V.; Yazdi, G. R.; Lashkarev, G.; Ulyashin, A.; Yakimova, R. Investigation of ZnO as a Perspective Material for Photonics. *Phys. Status Solidi A* **2008**, *205* (1), 144−149.
(8) Ozgur, U.; Alivov, Y. I.; Liu, C.; Teke, A.; Reshchikov, M. A.; Dogan, S.; Avrutin, V.; Cho, S. J.; Morkoc, H. A Comprehensive Review of ZnO Materials and Devices. *J. Appl. Phys.* **2005**, *98* (4), 041301.
(9) Baji, Z.; Lábadi, Z.; Horváth, Z. E.; Bársony, I. Structure and Morphology of Aluminium Doped Zinc-Oxide Layers Prepared by Atomic Layer Deposition. *Thin Solid Films* **2012**, *520* (14), 4703−4706.
(10) Banerjee, P.; Lee, W.-J.; Bae, K.-R.; Lee, S. B.; Rubloff, G. W. Structural, Electrical, and Optical Properties of Atomic Layer Deposition Al-Doped ZnO Films. *J. Appl. Phys.* **2010**, *108* (4), 445305.
(11) Cheun, H.; Fuentes-Hernandez, C.; Shim, J.; Fang, Y.; Cai, Y.; Li, H.; Sigdel, A. K.; Meyer, J.; Maibach, J.; Dindar, A.; et al. Oriented Growth of Al_2O_3:ZnO Nanolaminates for Use as Electron-Selective Electrodes in Inverted Polymer Solar Cells. *Adv. Funct. Mater.* **2012**, *22* (7), 1531−1538.
(12) Dasgupta, N. P.; Neubert, S.; Lee, W.; Trejo, O.; Lee, J.-R.; Prinz, F. B. Atomic Layer Deposition of Al-Doped ZnO Films: Effect of Grain Orientation on Conductivity. *Chem. Mater.* **2010**, *22* (16), 4769−4775.
(13) Geng, Y.; Guo, L.; Xu, S.-S.; Sun, Q.-Q.; Ding, S.-J.; Lu, H.-L.; Zhang, D. W. Influence of Al Doping on the Properties of ZnO Thin Films Grown by Atomic Layer Deposition. *J. Phys. Chem. C* **2011**, *115* (25), 12317−12321.
(14) Hu, Y. M.; Lin, C. W.; Huang, J. C. A. Dependences of the Al Thickness and Annealing Temperature on the Structural, Optical, and Electrical Properties in ZnO/Al Multilayers. *Thin Solid Films* **2006**, *497* (1−2), 130−134.
(15) Dallali, L.; Jaziri, S.; El Haskouri, J.; Amoros, P. Optical Properties of Exciton Confinement in Spherical ZnO Quantum Dots

Embedded in SiO_2 Matrix. *Superlattices Microstruct.* **2009**, *46* (6), 907−916.
(16) Kiliani, G.; Schneider, R.; Litvinov, D.; Gerthsen, D.; Fonin, M.; Rudiger, U.; Leitenstorfer, A.; Bratschitsch, R. Ultraviolet Photoluminescence of ZnO Quantum Dots Sputtered at Room-Temperature. *Opt. Express* **2011**, *19* (2), 1641−1647.
(17) Zeng, Z.; Paspalakis, E.; Garoufalis, C. S.; Terzis, A. F.; Baskoutas, S. Optical Susceptibilities in Singly Charged ZnO Colloidal Quantum Dots Embedded in Different Dielectric Matrices. *J. Appl. Phys.* **2013**, *113* (5), 054303.
(18) Dallali, L.; Jaziri, S.; el Haskouri, J.; Amorós, P.; Martínez-Pastor, J. Energy of Excitons and Acceptor−Exciton Complexes To Explain the Origin of Ultraviolet Photoluminescence in ZnO Quantum Dots Embedded in a SiO_2 Matrix. *Solid State Commun.* **2011**, *151* (11), 822−825.
(19) Marichy, C.; Bechelany, M.; Pinna, N. Atomic Layer Deposition of Nanostructured Materials for Energy and Environmental Applications. *Adv. Mater.* **2012**, *24* (8), 1017−1032.
(20) Elam, J. W.; George, S. M. Growth of ZnO/Al_2O_3 Alloy Films Using Atomic Layer Deposition Techniques. *Chem. Mater.* **2003**, *15* (4), 1020−1028.
(21) Elam, J. W.; Sechrist, Z. A.; George, S. M. ZnO/Al_2O_3 Nanolaminates Fabricated by Atomic Layer Deposition: Growth and Surface Roughness Measurements. *Thin Solid Films* **2002**, *414* (1), 43−55.
(22) Karvonen, L.; Säynätjoki, A.; Chen, Y.; Jussila, H.; Rönn, J.; Ruoho, M.; Alasaarela, T.; Kujala, S.; Norwood, R. A.; Peyghambarian, N.; et al. Enhancement of the Third-Order Optical Nonlinearity in ZnO/Al_2O_3 Nanolaminates Fabricated by Atomic Layer Deposition. *Appl. Phys. Lett.* **2013**, *103* (3), 031903.
(23) Wang, T.; Wu, H.; Chen, C.; Liu, C. Growth, Optical, and Electrical Properties of Nonpolar M-Plane ZnO on p-Si Substrates with Al_2O_3 Buffer Layers. *Appl. Phys. Lett.* **2012**, *100* (1), 011901.
(24) Mihailova, I.; Gerbreders, V.; Tamanis, E.; Sledevskis, E.; Viter, R.; Sarajevs, P. Synthesis of ZnO Nanoneedles by Thermal Oxidation of Zn Thin Films. *J. Non-Cryst. Solids* **2013**, *377*, 212−216.
(25) Elias, J.; Utke, I.; Yoon, S.; Bechelany, M.; Weidenkaff, A.; Michler, J.; Philippe, L. Electrochemical Growth of ZnO Nanowires on Atomic Layer Deposition Coated Polystyrene Sphere Templates. *Electrochim. Acta* **2013**, *110*, 387−392.
(26) Abou Chaaya, A.; Viter, R.; Bechelany, M.; Alute, Z.; Erts, D.; Zalesskaya, A.; Kovalevskis, K.; Rouessac, V.; Smyntyna, V.; Miele, P. Evolution of Microstructure and Related Optical Properties of ZnO Grown by Atomic Layer Deposition. *Beilstein J. Nanotechnol.* **2013**, *4*, 690−698.
(27) Marquez, J. A. R.; Rodriguez, C. M. B.; Herrera, C. M.; Rosas, E. R.; Angel, O. Z.; Pozos, O. T. Effect of Surface Morphology of ZnO Electrodeposited on Photocatalytic Oxidation of Methylene Blue Dye Part I: Analytical Study. *Int. J. Electrochem. Sci.* **2011**, *6* (9), 4059−4069.
(28) Reddy, A. J.; Kokila, M. K.; Nagabhushana, H.; Rao, J. L.; Shivakumara, C.; Nagabhushana, B. M.; Chakradhar, R. P. S. Combustion Synthesis, Characterization, and Raman Studies of ZnO Nanopowders. *Spectrochim. Acta, Part A* **2011**, *81* (1), 53−58.
(29) Holzwarth, U.; Gibson, N. The Scherrer Equation versus the "Debye-Scherrer Equation'. *Nat. Nanotechnol.* **2011**, *6* (9), 534−534.
(30) Yogamalar, N. R.; Chandra Bose, A. Absorption−Emission Study of Hydrothermally Grown Al:ZnO Nanostructures. *J. Alloys Compd.* **2011**, *509* (34), 8493−8500.
(31) Wang, N. W.; Yang, Y. H.; Yang, G. W. Great Blue-Shift of Luminescence of ZnO Nanoparticle Array Constructed from ZnO Quantum Dots. *Nanoscale Res. Lett.* **2011**, *6*, 338.
(32) Charpentier, C.; Prod'homme, P.; Cabarrocas, P. R. I. Microstructural, Optical, and Electrical Properties of Annealed ZnO:Al Thin Films. *Thin Solid Films* **2013**, *531*, 424−429.
(33) Barker, A. S. Infrared Lattice Vibrations and Dielectric Dispersion in Corundum. *Phys. Rev.* **1963**, *132* (4), 1474−1481.
(34) Dai, Z.-H.; Zhang, R.-J.; Shao, J.; Chen, Y.-M.; Zheng, Y.-X.; WU, J.-D.; Chen, L.-Y. Optical Properties of Zinc-Oxide Films Determined Using Spectroscopic Ellipsometry with Various Dispersion Models. *J. Korean Phys. Soc.* **2009**, *55*, 1227−1232.
(35) Nguyen, H. V.; An, I.; Collins, R. W. Evolution of the Optical Functions of Thin-Film Aluminum: A Real-Time Spectroscopic Ellipsometry Study. *Phys. Rev. B: Condens. Matter* **1993**, *47* (7), 3947−3965.
(36) Leng, J. M.; Chen, J.; Fanton, J.; Senko, M.; Ritz, K.; Opsal, J. Characterization of Titanium Nitride (TiN) Films on Various Substrates Using Spectrophotometry, Beam Profile Reflectometry, Beam Profile Ellipsometry, and Spectroscopic Beam Profile Ellipsometry. *Thin Solid Films* **1998**, *313−314* (0), 308−313.
(37) Talbot, D. R. S.; Willis, J. R.; Nesi, V. On Improving the Hashin−Shtrikman Bounds for the Effective Properties of Three-Phase Composite Media. *IMA J. Appl. Math.* **1995**, *54* (1), 97−107.
(38) Yakuphanoglu, F.; Ilican, S.; Caglar, M.; Caglar, Y. The Determination of the Optical Band and Optical Constants of Non-Crystalline and Crystalline ZnO Thin Films Deposited by Spray Pyrolysis. *J. Optoelectron. Adv. Mater.* **2007**, *9*, 2180−2185.
(39) Miao, L.; Tanemura, S.; Zhao, L.; Xiao, X.; Zhang, X. T. Ellipsometric Studies of Optical Properties of Er-Doped ZnO Thin Films Synthesized by Sol−Gel Method. *Thin Solid Films* **2013**, *543* (0), 125−129.
(40) Benzarouk, H.; Drici, A.; Mekhnache, M.; Amara, A.; Guerioune, M.; Bernède, J. C.; Bendjffal, H. Effect of Different Dopant Elements (Al, Mg, and Ni) on Microstructural, Optical, and Electrochemical Properties of ZnO Thin Films Deposited by Spray Pyrolysis (SP). *Superlattices Microstruct.* **2012**, *52* (3), 594−604.
(41) Xue, S. W.; Zu, X. T.; Zheng, W. G.; Deng, H. X.; Xiang, X. Effects of Al Doping Concentration on Optical Parameters of ZnO: Al Thin Films by Sol−Gel Technique. *Phys. B* **2006**, *381* (1−2), 209−213.
(42) Cho, E. N.; Park, S.; Yun, I. Spectroscopic Ellipsometry Modeling of ZnO Thin Films with Various O_2 Partial Pressures. *Curr. Appl. Phys.* **2012**, *12* (6), 1606−1610.
(43) Fang, Z. B.; Yan, Z. J.; Tan, Y. S.; Liu, X. Q.; Wang, Y. Y. Influence of Post-Annealing Treatment on the Structure Properties of ZnO Films. *Appl. Surf. Sci.* **2005**, *241* (3−4), 303−308.
(44) Krishna, M. G.; Rao, K. N.; Mohan, S. Optical Properties of Ion Assisted Deposited Zirconia Thin Films. *J. Vac. Sci. Technol., A* **1992**, *10* (6), 3451−3455.
(45) Jin, B. J.; Woo, H. S.; Im, S.; Bae, S. H.; Lee, S. Y. Relationship Between Photoluminescence and Electrical Properties of ZnO Thin Films Grown by Pulsed Laser Deposition. *Appl. Surf. Sci.* **2001**, *169−170* (0), 521−524.
(46) Zandi, S.; Kameli, P.; Salamati, H.; Ahmadvand, H.; Hakimi, M. Microstructure and Optical Properties of ZnO Nanoparticles Prepared by a Simple Method. *Phys. B* **2011**, *406* (17), 3215−3218.
(47) Ábrahám, N.; Dékány, I. Size-Dependent Photoluminescence Properties of Bare ZnO and Polyethylene Imine Stabilized ZnO Nanoparticles and Their Langmuir−Blodgett Films. *Colloids Surf., A* **2010**, *364* (1−3), 26−33.
(48) Omata, T.; Takahashi, K.; Hashimoto, S.; Maeda, Y.; Nose, K.; Otsuka-Yao-Matsuo, S.; Kanaori, K. UV Luminescent Organic-Capped ZnO Quantum Dots Synthesized by Alkoxide Hydrolysis with Dilute Water. *J. Colloid Interface Sci.* **2011**, *355* (2), 274−281.
(49) Cui, L.; Wang, G.-G.; Zhang, H.-Y.; Sun, R.; Kuang, X.-P.; Han, J.-C. Effect of Film Thickness and Annealing Temperature on the Structural and Optical Properties of ZnO Thin Films Deposited on Sapphire (0001) Substrates by Sol−Gel. *Ceram. Int.* **2013**, *39* (3), 3261−3268.
(50) Giri, P. K.; Bhattacharyya, S.; Chetia, B.; Kumari, S.; Singh, D. K.; Iyer, P. K. High-Yield Chemical Synthesis of Hexagonal ZnO Nanoparticles and Nanorods with Excellent Optical Properties. *J. Nanosci. Nanotechnol.* **2012**, *12* (1), 201−206.
(51) Wang, Q. P.; Zhang, D. H.; Xue, Z. Y.; Hao, X. T. Violet Luminescence Emitted from ZnO Films Deposited on Si Substrate by rf Magnetron Sputtering. *Appl. Surf. Sci.* **2002**, *201* (1−4), 123−128.
(52) Djurišić, A. B.; Leung, Y. H. Optical Properties of ZnO Nanostructures. *Small* **2006**, *2* (8−9), 944−961.

(53) Willander, M.; Nur, O.; Sadaf, J. R.; Qadir, M. I.; Zaman, S.; Zainelabdin, A.; Bano, N.; Hussain, I. Luminescence from Zinc Oxide Nanostructures and Polymers and Their Hybrid Devices. *Materials* **2010**, *3* (4), 2643−2667.
(54) Chen, H.; Ding, J.; Guo, W.; Shi, F.; Li, Y. Violet−Blue−Green Emission and Shift in Mg-Doped ZnO films with Different Ratios of Oxygen to Argon Gas Flow. *Appl. Surf. Sci.* **2012**, *258* (24), 9913−9917.
(55) Liang, Z.; Yu, X.; Lei, B.; Liu, P.; Mai, W. Novel Blue-Violet Photoluminescence from Sputtered ZnO Thin Films. *J. Alloys Compd.* **2011**, *509* (17), 5437−5440.